Bridging the Gap: Capturing the Lyα Counterpart of a Type-II Spicule and Its Heating Evolution with VAULT2.0 and *IRIS* Observations

Georgios Chintzoglou[1,5] , Bart De Pontieu[1,6] , Juan Martínez-Sykora[1,7] , Tiago M. D. Pereira[2,6] ,
Angelos Vourlidas[3,8] , and Samuel Tun Beltran[4]

[1] Lockheed Martin Solar and Astrophysics Laboratory, 3176 Porter Drive, Palo Alto, CA 94304, USA; gchintzo@lmsal.com
[2] Rosseland Centre for Solar Physics, University of Oslo, P.O. Box 1029 Blindern, NO-0315 Oslo, Norway
[3] The Johns Hopkins University Applied Physics Laboratory, Laurel, MD 20723, USA
[4] Space Science Division, Naval Research Laboratory, Washington, DC 20375, USA

Abstract

We present results from an observing campaign in support of the VAULT2.0 sounding rocket launch on 2014 September 30. VAULT2.0 is a Lyα (1216 Å) spectroheliograph capable of providing spectroheliograms at high cadence. Lyα observations are highly complementary to the *IRIS* observations of the upper chromosphere and the low transition region (TR) but have previously been unavailable. The VAULT2.0 data provide new constraints on upper-chromospheric conditions for numerical models. The observing campaign was closely coordinated with the *IRIS* mission. Taking advantage of this simultaneous multi-wavelength coverage of target AR 12172 and by using state-of-the-art radiative-MHD simulations of spicules, we investigate in detail a type-II spicule associated with a fast (300 km s^{-1}) network jet recorded in the campaign observations. Our analysis suggests that spicular material exists suspended high in the atmosphere but at lower temperatures (seen in Lyα) until it is heated and becomes visible in TR temperatures as a network jet. The heating begins lower in the spicule and propagates upwards as a rapidly propagating thermal front. The front is then observed as fast, plane-of-the-sky motion typical of a network jet, but contained inside the pre-existing spicule. This work supports the idea that the high speeds reported in network jets should not be taken as real mass upflows but only as apparent speeds of a rapidly propagating heating front along the pre-existing spicule.

Key words: Sun: chromosphere – Sun: general – Sun: transition region – Sun: UV radiation

Supporting material: animation

1. Introduction

The chromosphere is one of the least understood layers of the solar atmosphere because of our limited understanding of the governing physical processes. In the last 10 to 15 years, the chromosphere has been propelled to the forefront of solar physics research thanks to spectacular new observations from space with the Solar Optical Telescope (SOT; Tsuneta et al. 2008) on board the *HINODE* spacecraft, the *Interface Region Imaging Spectrograph* (*IRIS*; De Pontieu et al. 2014), the Very high Angular resolution Ultraviolet Telescope (VAULT; Korendyke et al. 2001), and from the ground with the Dutch Open Telescope (Rutten et al. 2004), the Interferometric Bidimensional Spectropolarimeter (IBIS; Cavallini 2006), the 1 m Swedish Solar Telescope (SST; Scharmer et al. 2003), and, particularly, the CRisp Imaging Spectro-Polarimeter (Scharmer et al. 2008). The advent of sophisticated numerical simulations, which are beginning to address the complex physics of the optically thick chromospheric plasmas, has helped in the interpretation of the observations (e.g., Martínez-Sykora et al. 2017b).

A new class of spicules (type-II spicules) has been discovered in *Hinode*/SOT Ca II H observations (De Pontieu et al. 2007). They seem to exhibit much faster speeds as compared to the "traditional" class of type-I spicules (50–100 km s^{-1}). In Ca II H filtergrams, type-II spicules appear to be shorter lived (with typical lifetimes of 10–150 s) than type-I spicules, whereas, for higher chromospheric temperatures (e.g., Mg II h and k formation temperatures) or transition region (TR) temperatures (e.g., Si IV), the lifetimes are 3–10 minutes (Pereira et al. 2014). These spicules are rooted in the chromospheric network and consequently, due to their ubiquity, they are regarded as a significant source of coronal mass and heat transfer (De Pontieu et al. 2009). Tian et al. (2014) studied counterparts to spicules in the *IRIS* FUV SJI channels and called them "network jets." They measured the plane-of-the-sky speeds with the aid of space–time plots and reported speeds of ≈80–250 km s^{-1}. They concluded that due to these very fast speeds, network jets could be a significant source of mass to the solar wind. On the other hand, Rouppe van der Voort et al. (2015), using SST and *IRIS* observations, studied the heating signatures of on-disk type-II spicules and they found that many type-II spicules on the disk are associated with network jets. In addition, they provided Doppler speeds of these on-disk type-II spicules. These speeds (50–75 km s^{-1}) seem to disagree with the speeds of Tian et al. (2014), despite the similar viewing angles. This discrepancy raises the important question of whether the high speeds reported by Tian et al. (2014) are apparent speeds and not true mass upflows. De Pontieu et al. (2017) used the state-of-the-art simulations of Martínez-Sykora et al. (2017b) and suggested that the speeds of the network jets are likely not caused by real mass motions, but by heating fronts that propagate at those

speeds. The network jet speeds would then be understood as apparent speeds (and not real mass motions). This can resolve the discrepancy between the plane-of-the sky motions in images and the line-of-sight velocities from Doppler measurements.

In this paper, we derive new observational constraints from the VAULT2.0 and *IRIS* coordinated observations. The VAULT2.0 rocket experiment (Very high Angular resolution Ultraviolet Telescope 2.0; Vourlidas et al. 2016) is a Lyα spectroheliograph designed to observe the upper-chromospheric region of the solar atmosphere in high spatial (∼1″) and temporal resolution (8 s). VAULT2.0 is a reflight of the VAULT rocket and was successfully launched on 2014 September 20 from White Sands Missile Range. The VAULT2.0 experiment was complemented by an observing "campaign" from ground-based (BBSO, IBIS/NSO, SOLIS) and space-borne (*SDO*/AIA/HMI, *IRIS*, *HINODE*/EIS/SOT) observatories. The importance of the addition of VAULT2.0 Lyα observations is that Lyα is formed at a location in the spectrum where the UV continuum is low, essentially allowing imaging with relatively low photospheric contamination and thus high contrast due to suppressed background emission. This is critical when seeking the on-disk counterparts of type-II spicules.

This paper is organized as follows: in Section 2, we describe the joint VAULT2.0 and *IRIS* observations of a type-II spicule. In Section 3, we discuss the numerical model used to interpret the observations followed by a discussion in Section 4. We conclude in Section 5.

2. Campaign Observations

The VAULT2.0 observing window lasted for about five minutes (18:09–18:14 UT). However, the campaign observations were initiated several hours before and concluded a few hours after the VAULT2.0 flight. During its flight, VAULT2.0 observed a failed eruption and captured cooling downflows and bright ribbons around the target AR 12172 (Chintzoglou et al. 2017). At the time of the flight, the AR was at heliographic coordinates S15° W55°. The VAULT2.0 large (384″ × 256″) field of view (FOV) captured substantial areas of the quiet Sun (QS) around the target AR. The spatial resolution was determined post flight (≲1″2; Vourlidas et al. 2016) and 34 images were recorded at an 8 s cadence.

IRIS supported the observational campaign by providing a fast time-cadence (13 s) image series from its slit-jaw imagers (in short, SJI). *IRIS* was in a "sparse" (1″ separation) eight-step raster mode (OBS-ID 3820255277), centered at $(x, y) = (711″, -281″)$ and observed the target between 17:13 and 20:04 UT. The SJI passbands covered the lower TR at 1400 Å (dominated by Si IV ion emission) and at 1330 Å (dominated by C II ion emission) with mean formation temperatures of ≈80,000 K and ≈30,000 K respectively (see Rathore & Carlsson 2015 for a further discussion on the dominant temperatures of plasma emission in C II 1330 Å). The FOV of these *IRIS* SJI images (120″ × 120″) is smaller than that of VAULT2.0, but large enough to contain the core of the target AR as well as some QS region north and south of the AR. The SJI pixel size is 0″167 pix^{-1} and the data were corrected for flat-field, dark current, and geometric distortions as described in De Pontieu et al. (2014). In Figure 1, we show the FOVs of each instrument superimposed on a 304 Å context image from the Atmospheric Imaging Assembly (AIA; Lemen et al. 2012) on board the *Solar Dynamics Observatory* (*SDO*; Pesnell et al. 2012).

Qualitatively, the Lyα observations show similarities in structure with observations in the 304 Å passband of *SDO*/AIA and also with the SJI 1400 and 1330 Å passbands of *IRIS* (compare panels (a) and (b) of Figure 1). In the QS, the chromospheric network is the dominant structure, while in the location of the AR an inverse U-shape filament is seen as a dark feature, surrounded by emission from the nearby plage.

Since the campaign includes only on-disk observations, we restricted our efforts in finding type-II spicules on-disk. This restriction, combined with the relatively small *IRIS* SJI FOV, made for a challenging analysis since spicules are best seen against low background emission (which is best for spicules at the limb). After carefully inspecting the image series in the common FOV of VAULT2.0 and *IRIS* for spicules, we identified a fast network jet in the *IRIS* 1400 and 1330 Å passbands in the south of AR 12172 (the location is shown with a green box in Figure 1). In Figure 2, we show three snapshots of the area around the network jet, as recorded in the aforementioned VAULT2.0 and *IRIS* passbands. The 20″ × 30″ FOV contains chromospheric material with both dark and bright features (see Figure 1). These features form a darker background against which a sudden brightening, typical of a network jet, can be identified on-disk. The network jet is shown in the bottom right panel of Figure 2 (indicated with a white arrow). Based on the SJI images, the width of the jet is found to be ∼0″5.

The space–time plot of Figure 3 shows a parabolic profile (visible in both *IRIS* passbands but best seen in Si IV 1400 Å due to its better signal-to-noise ratio). This is compatible with the presence of a type II spicule, with the bright TR emission outlining the spatial extent of the spicular material, as is also shown in De Pontieu et al. (2017). This may be associated with a heating front at TR temperatures as it travels along the spicule's axis (Martínez-Sykora et al. 2017b). When the spicule is fully evolved (∼40 s later), it brightens along its whole length (18:13:08 UT) in the 1400 and 1330 Å SJI images. Emission reoccurs about a minute after the first peak of emission, at 18:14:40 UT. This resurgence leaves two almost vertical streaks in the space–time plot of 1400 and 1330 Å in Figure 3. Their vertical extent corresponds to the length of the spicule, ∼4 Mm projected on the plane of the sky. From these space–time plots, we deduce an apparent speed of ∼300 km s^{-1}.

The VAULT2.0 observations reveal a slighlty different behavior than the *IRIS* observations. Lyα emission peaks simultaneously with the Si IV 1400 Å and C II 1330 Å emission as shown in the space–time plots of Figure 3. However, while the apparent parabolic profiles in the *IRIS* passbands develop, there is sudden Lyα emission over the full length of the spicule for up to 120 s before the first brightening in 1400 and 1330 Å at 18:13:48 UT (emission between the 18:12 and 18:14 vertical bar, top left panel in Figure 3). The feature can be seen in the VAULT2.0 frame in the middle top panel of Figure 2 (red dashed circle). In addition, the Lyα structure has the same linear extent as the *IRIS*-observed type-II spicule, which suggests that material appears to pre-exist at the location where the network jet occurs, but at temperatures lower than the TR temperatures observed by *IRIS*.

The measured plane-of-the-sky speed of ∼300 km s^{-1} lies on the high-end of the speeds of network jets reported by Tian et al. (2014) and Narang et al. (2016). In this particular case, the brightening is happening in a spicule in an active region. In
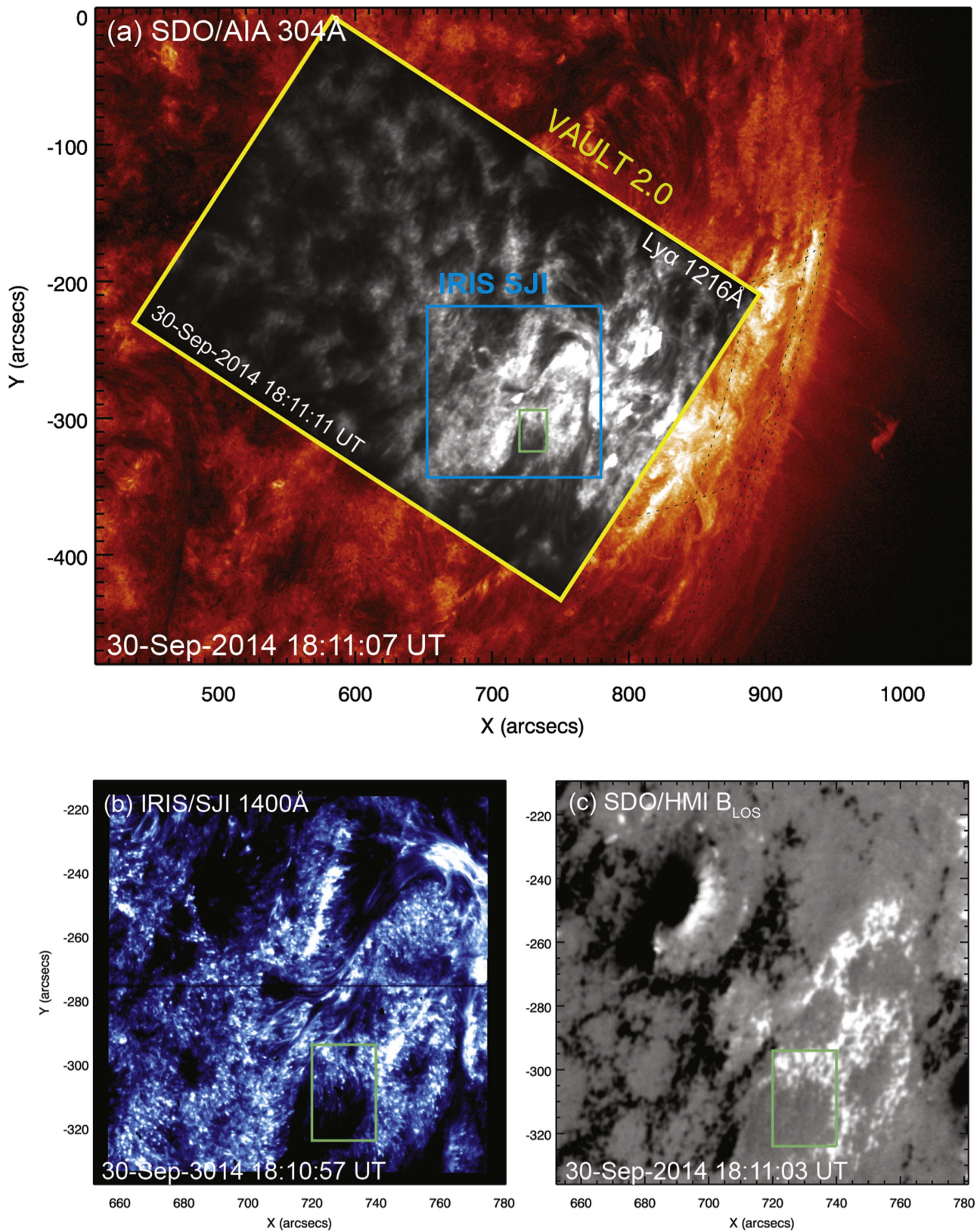
Figure 1. (a) Context image from AIA/*SDO* at 304 Å, showing the FOV of VAULT2.0 and *IRIS*. The green box shows a region of $20'' \times 30''$ centered at the location of the Type-II spicule co-observed by VAULT2.0 and *IRIS*. (b) The FOV of *IRIS* SJI in 1400 Å. (c) The line-of-sight magnetogram from HMI/*SDO* for the FOV of panel (b) saturated at ± 500 G. Light (dark) tones of gray correspond to positive (negative) magnetic polarities. The location where the type-II spicule and network jet occur (green box) is adjacent to a positive polarity plage region.
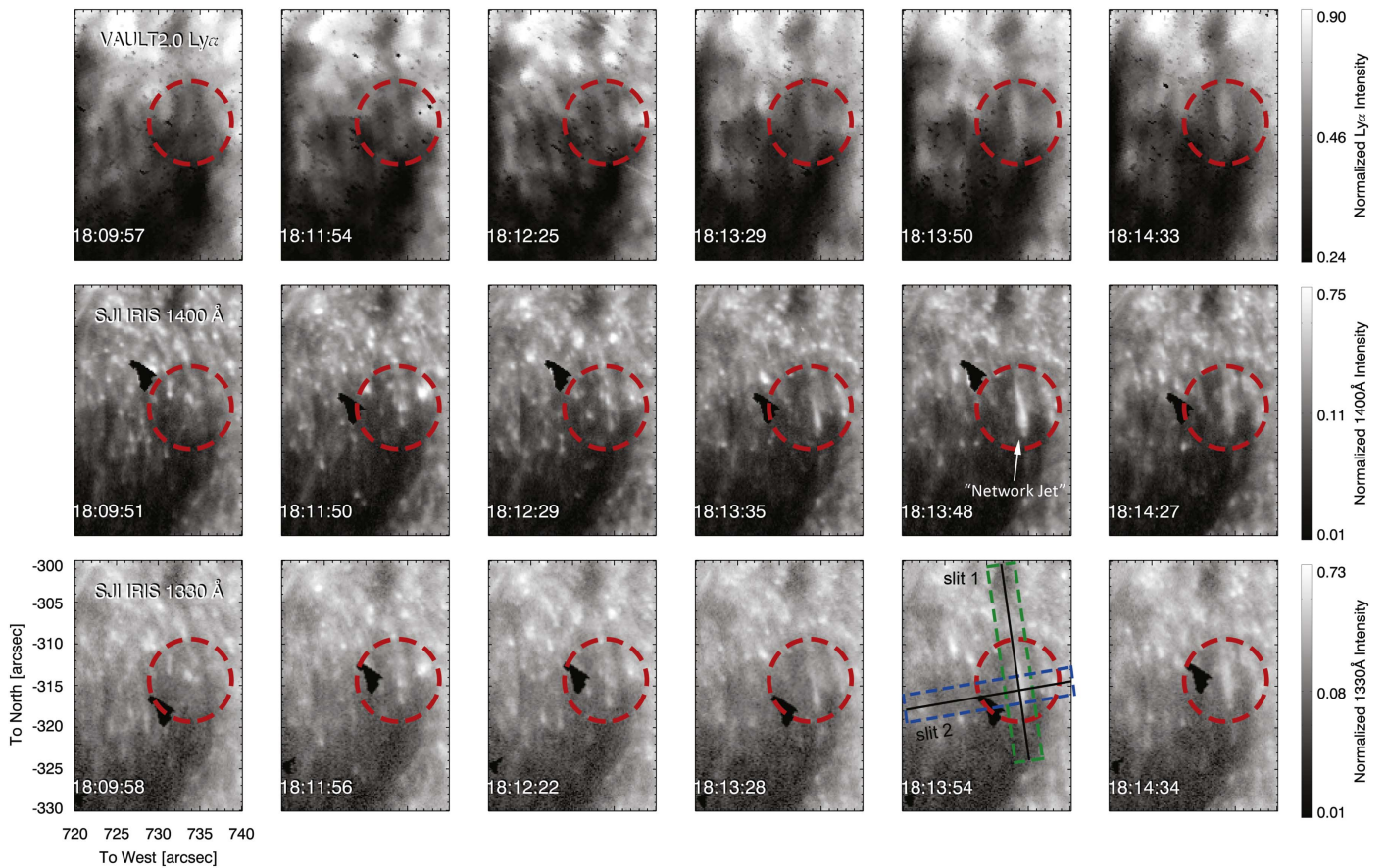
Figure 2. Time-evolution of a network jet observed in Lyα 1216 Å by VAULT2.0 (top row) and with the *IRIS* slit-jaw imager in Si IV 1400 Å (middle row) and C II 1330 Å (bottom row). The FOV corresponds to the green box of Figure 1. Intensities for each passband *I* are normalized as *I/I*max with *I*max being the strongest intensity in the FOV of the entire time series. Scaling is logarithmic (base 10) for all panels. The sharp dark features in the *IRIS* FOVs are particles on the slit-jaw detector. The network jet occurs at the time shown in the last columns of Si IV 1400 Å and C II 1330 Å. The Lyα counterpart of the network jet is shown inside the red dashed circle in the top row and it seems to pre-exist (at least in the panel at 18:11:54 UT) the appearance of the network jet (compare the content in red dashed circles between wavelengths). The green dashed rectangle shown in panel 18:13:54 marks the area containing the network jet and the blue dashed rectangle marks the area intersecting the network jet at approximately a 90° angle. Pixels along the dark lines inside these locations are used in the space–time plots of Figure 3.

the following section, we investigate this case with an advanced radiative-MHD model.

3. Bifrost Model of a Spicule

To address the questions raised by our analysis, we compare the observations to simulated spicules (Martínez-Sykora et al. 2017b). The Bifrost code (Gudiksen et al. 2011) solves the MHD equations, while including the radiative losses (Hayek et al. 2010; Carlsson & Leenaarts 2012), the thermal conduction along the magnetic field, and the ion-neutral interaction effects by adding the ambipolar diffusion and the Hall term in the induction equation (see Martínez-Sykora et al. 2012, 2017a for details on the ambipolar diffusion on these models). This model solves the single-fluid MHD equations and takes into account ion-neutral interaction effects. In short, in a partially ionized magnetized gas, the ambipolar diffusion describes the decoupling of the bulk of the fluid with magnetic flux. This is a consequence of neutrals being able to move "freely," while ions are coupled to the magnetic field. Due to collisions, ions can also be decoupled from the magnetic field. Note that the ambipolar diffusion permits the diffusion of the magnetic field and dissipates magnetic energy into thermal energy. This numerical model is capable of self-consistently producing type-II spicules (Martínez-Sykora et al. 2017b).

The simulation analyzed here is the 2.5D radiative-MHD model described in detail in Martínez-Sykora et al. (2016, 2017b). The numerical domain ranges from the upper layers of the convection zone (3 Mm below the photosphere) to the self-consistently maintained hot corona (40 Mm above the photosphere) and 90 Mm along the horizontal axis. The spatial resolution is 14 km along the horizontal axis. For the vertical direction, the grid is non-uniform, allowing for a finer grid size in locations where it is necessary to resolve features, such as in the photosphere to the TR, and coarser in the corona and deeper into the convection zone (i.e., variable grid size ranging from 12–50 km). This simulation shows the formation of very fast network jets seen in synthesized Si IV emission (De Pontieu et al. 2017). In addition, we derive synthetic Lyα observables to interpret the thermal evolution from the observations.

For this work, we calculated the synthetic Si IV intensity, assuming ionization equilibrium and an optically thin approximation, such as that in Hansteen et al. (2010). Lyα profiles were calculated in detail by solving the full non-LTE radiative transfer problem on a column by column basis with the RH 1.5D code (Uitenbroek 2001; Pereira & Uitenbroek 2015). A five-level plus continuum model hydrogen atom was used. The 1.5D approximation was used to keep the computational costs down. To compare with VAULT2.0 observations, we integrated the synthetic Lyα line profiles over a Gaussian bandpass
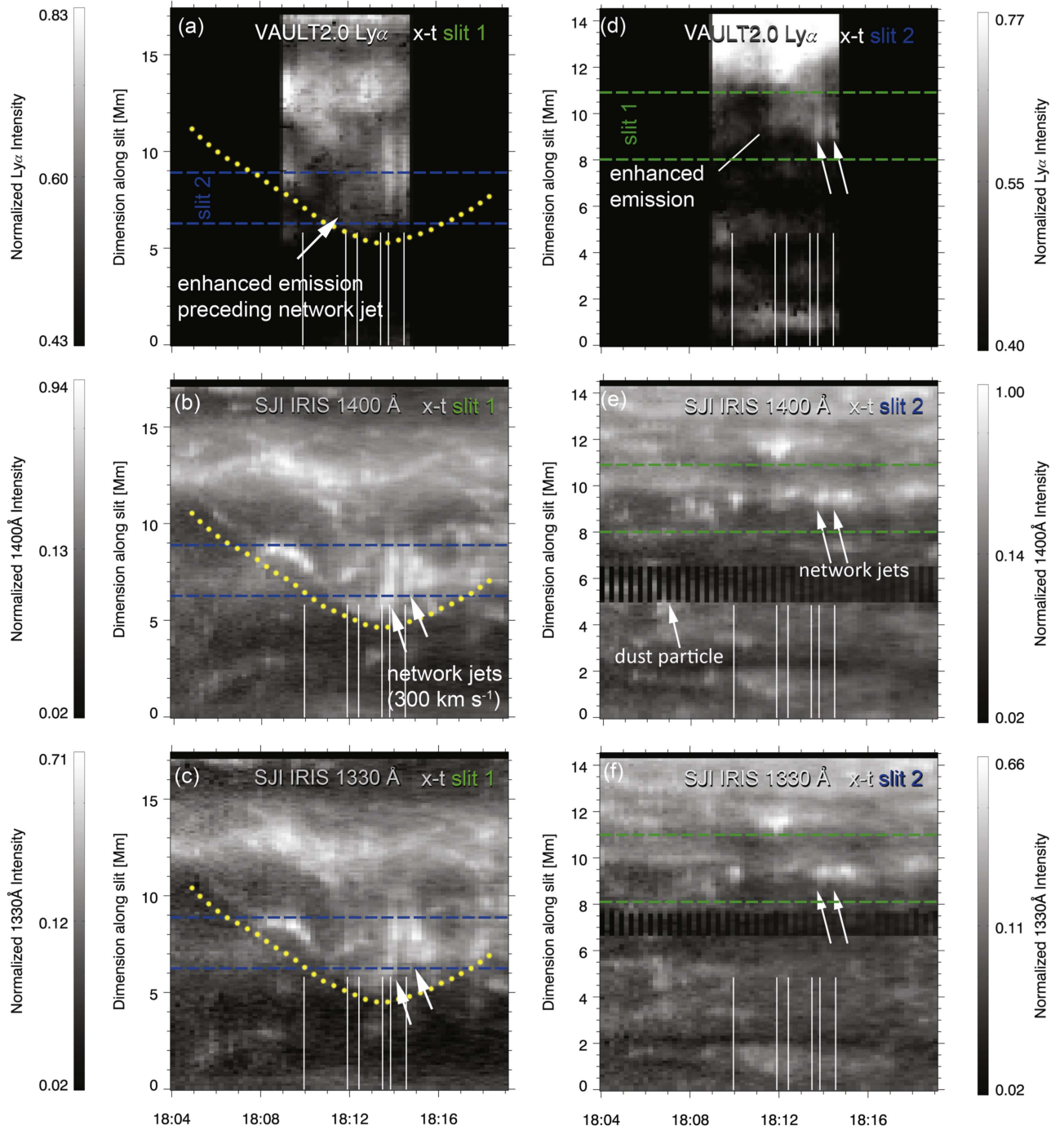
Figure 3. Space–time plots composed for all wavelengths for slits 1 and 2 shown in Figure 2 (panel at 18:13:54). Left panels (a)–(c) show the evolution of the brightenings along slit 1 for each passband and the right panels show the evolution along slit 2, i.e., at a cross-section with the network jet. To guide the eye with reference to Figure 2, we show the intersection of the rectangular area of slit 2 with slit 1 as blue dashed lines. Similarly, in the right panels, we show with green dashed lines the area around slit 1 as intersected by slit 2 (containing the cross-section of the network jet once it occurs). Intensity scaling is logarithmic (base 10). Times when VAULT2.0 was not observing are shown in black. The bottom part of the spicule is at the top of the slit. In the 1400 and 1330 Å space–time plots, we see that the type II spicule manifests itself in the form of a parabolic trace (yellow dotted curve superposed in all left panels for reference). The spicule seems to undergo a recurring second brightening along its length 40 s after the first brightening, also shown in 1216 Å. The selected times of the panels in Figure 2 are shown with white vertical lines. The type-II spicule in Lyα shows emission preceding the sudden brightening/network jets seen in *IRIS* by almost two minutes (panel (a); arrow pointing to the location above the parabolic trace). An animation showing the dynamics of the event is also available. The space–time plots produced from slits 1 and 2 appear in the middle and right columns of the animation, while the left column shows the slits superimposed on the FOV shown in Figure 2 for each passband. The times begin(end) at 18:09:05(18:14:43), 18:08:58(18:14:40), and 18:09:05(18:14:47) for the Lyα, 1400, and 1330 Å passbands respectively.

(An animation of this figure is available.)

with 80 Å FWHM. Because of this integration, the mean intensity is more important than the spectral line shapes. While Lyα suffers from partial redistribution (PRD) effects (Milkey &

Mihalas 1973), after testing a single snapshot from our model series, we find that when using the 1.5D approximation, calculations assuming complete redistribution (CRD) give a
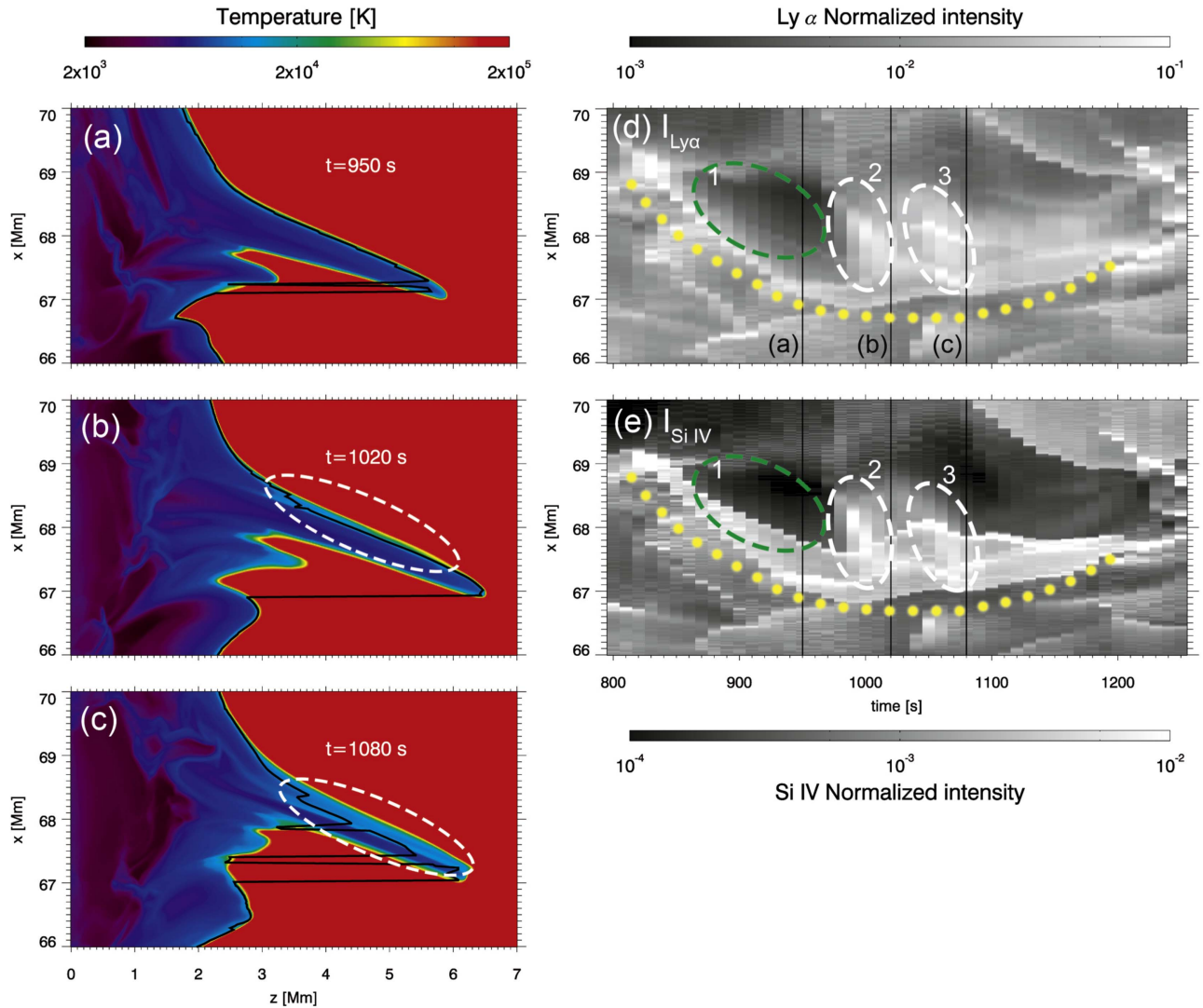
Figure 4. Panels (a)–(c): temperature maps for a simulated type-II spicule at three time instances (shown with black lines in panels (d) and (e)). The horizontal dimension, x, is placed in the vertical axis to account for a spicule that grows southward (as in the observations). The photospheric surface is at $z = 0$. The black curve shows the height of $\tau = 1$ for the peak intensity of Lyα for an observer viewing from the top-down toward the solar surface (in this arrangement of the maps, the observer's view is from right to left). While spicular material is already suspended up to 6 Mm from the photosphere, Lyα emission comes from different parts along the spicule as it heats up. Panels (d)–(e): Lyα and Si IV space–time plots of their normalized emergent intensities, I/I_{max} with I_{max} the strongest intensity in the entire time series. The spatial axis is the vertical axis in (a)–(c) panels. The intensity scaling in all panels is logarithmic (base 10). Note the parabolic trace left in the space–time plots due to the evolving spicule (yellow dotted curve). Note the higher normalized intensity of Lyα as compared to Si IV (inside the green dashed oval 1; before the first network jet). The occurence of the network jets is marked with white dashed ovals 2 and 3 (see the text).

mean intensity that is closer to the full 3D PRD approach. The reason is that the PRD effects reduce the intensity in the line wings, while 3D effects do the opposite (Sukhorukov & Leenaarts 2017). Therefore, our adopted 1.5D CRD approach gives a reasonable approximation when studying wavelength-integrated Lyα profiles.

In Figure 4, we present temperature maps from the simulation at three consecutive instances during the heating of the type-II spicule (panels (a)–(c)) and synthesized Lyα and Si IV emergent intensities in space–time plots (as observed from the top of the box). Similarly to the observations in Si IV, a bright point-like front travels with the growing spicule as seen in the space–time plots (forming a parabolic profile; yellow dotted envelope in panels (d) and (f)). This arises from a moving front of TR emission at the top of the spicule (panel (a)), enhancing the emissivity in both simulated passbands (Lyα and Si IV). However, up to that time, in the region enclosed by the yellow

dotted parabolic envelope (inside the green dashed oval 1 in panels (d) and (e)), there seems to be an order of magnitude difference in the normalized intensities between Lyα and Si IV, with Lyα emission being higher than Si IV. This enhanced emissivity of Lyα comes from the spicular column (above $\tau = 1$), similarly to the enhanced emission seen in the observed Lyα space–time profile before the occurrence of the network jet in Si IV (panels (a) and (b) in Figure 3). Then, at ∼990 s, a sudden brightening occurs along the whole spicule in Si IV (and Lyα) caused by a sudden temperature increase (up to ∼10^4 K) in a very narrow region on the right-hand side of the spicule (panel (b)). This corresponds to the bright linear feature inside of the dashed oval 2 in the space–time plots in panels (d) and (e).

In the temperature panels, the formation height of Lyα ($\tau = 1$, shown by the black solid lines in panels (a)–(c)) is at the exact location of the region that undergoes the temperature increase (dashed oval, panel (b)). Around 70 s later ($t = 1080$ s; dashed
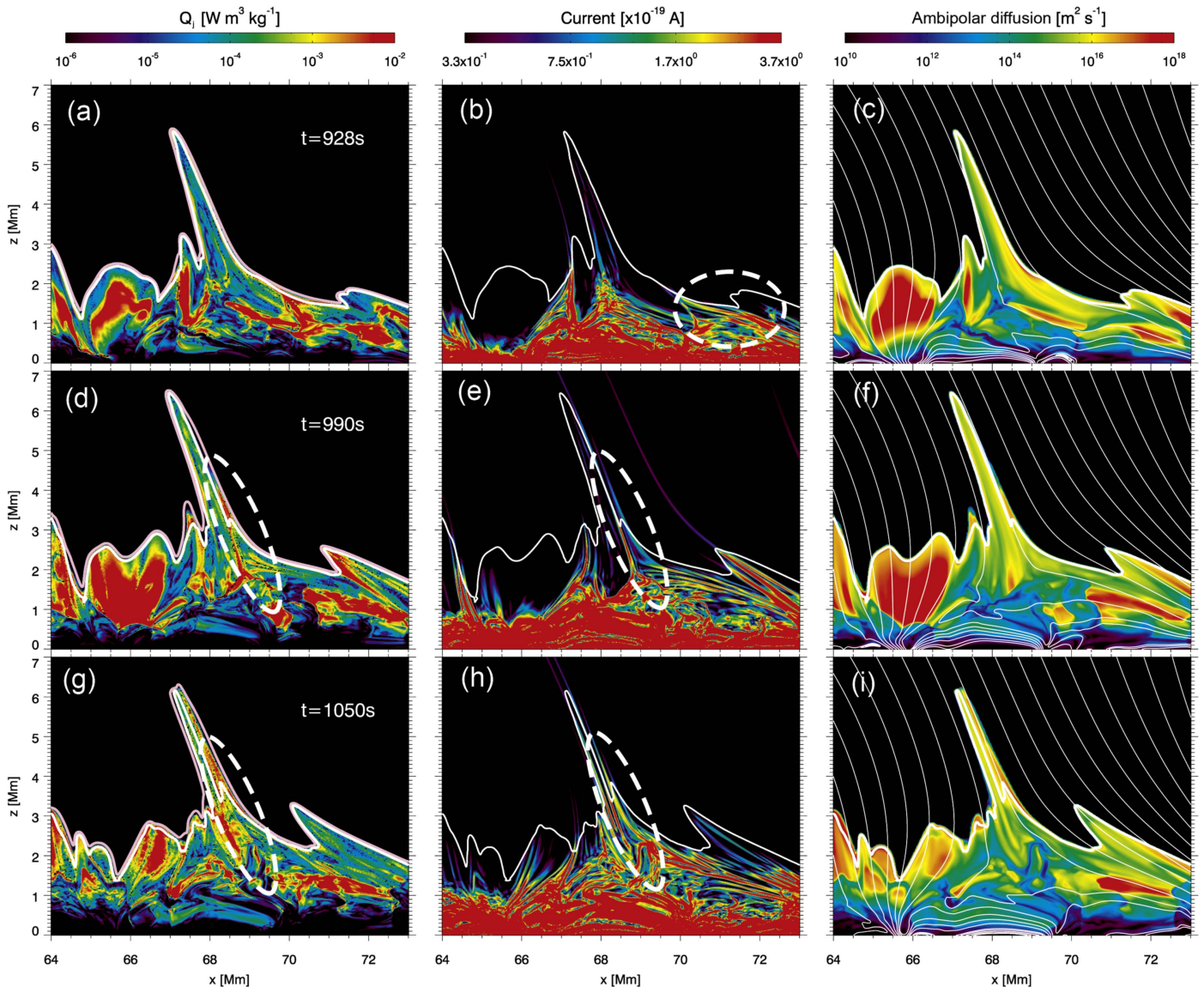
Figure 5. Joule heating, Q_j, the magnitude of electrical current, $|J|$, and ambipolar diffusion for the Type-II spicule of Figure 4 arranged in columns at three time instances of the simulation (rows at $t = 928$, 990, and 1050 s). The thick white (all panels) and pink (left) lines show $T = 10^4$ K and $T = 10^5$ K isocontours, respectively. Selected magnetic field lines are shown in the right panels (thin white lines). Note the evolution of ambipolar diffusion and the electrical currents with the receding temperature isocontour over time. At $t = 928$ s, electric currents between $x = 71$–73 Mm intensify (panel (b); white dashed oval) and at $t = 990$ s extend radially outward along the spicule (dashed oval in panel (e)), increasing the Joule heating and subsequently the temperature of the outer part of the spicule (dashed ovals in panels (d) and (g)).

oval 3 in space–time plots in panels (d) and (e)), a second emission enhancement occurs that is associated with an increase of temperature up to $\sim 10^4$ K in most of the spicular plasma (panel (c), dashed oval).

To further investigate the physical processes responsible for the simulated event, we explored the Joule Heating (left column, Figure 5), electrical current ($|J|$, middle), and ambipolar diffusion (right) at selected times before the times of the panels (a)–(c) of Figure 4. An electrical current is traveling within the chromosphere (directed from right to left, as seen in Figure 4) at Alfvénic speeds. At $t = 928$ s, the current front is at $x \approx 70.8$ Mm (shown with a dashed oval in panel (b)) and at $t = 990$ s has spread out along the very right-hand side of the spicule (inside the oval in panel (e)). Due to ambipolar diffusion (Figure 5, right column) the current is dissipated rapidly and heats the plasma (left panels) in a very localized region along the spicule. The heating timescale of a

few seconds is a result of the rapid propagation and of the rapid dissipation of the currents, i.e., at an Alfvén speed between 300 and 500 km s^{-1}. Following this Alfvénic wave, a wider current front is covering most of the spicule at $t = 1050$ s.

4. Discussion

The existence of material in Lyα temperatures before the manifestation of network jets challenges the idea that the plane-of-the-sky motions of network jets are real mass motions of spicules seen in the TR. Previously, Tian et al. (2014) and Narang et al. (2016) performed a statistical study of a large sample of network jets seen in *IRIS* C II by measuring the plane-of-the-sky speeds and they found a distribution of speeds between 80 and 300 km s^{-1}. Rouppe van der Voort et al. (2015), conducted an analysis of the heating signatures of on-disk type-II spicules using Hα data from the SST with Si IV and

C II from *IRIS*. In their work, they reported Doppler velocities much lower than those in Tian et al. (2014), i.e., 50–75 km s^{-1}. We should stress here that both studies dealt with on-disk cases of network jets and type-II spicules, with similar viewing angles. The difference in the reported speeds between the two studies is striking. One would expect a close match of speeds deduced by the two methods (i.e., plane-of-the-sky speeds and Doppler-deduced speeds) if those motions were real mass motions. If there are real mass motions of ∼150–300 km s^{-1} then, given that network jets are observed to be roughly radially oriented, then the Doppler speeds should reveal these speeds or at least show an order of magnitude agreement. The observations from VAULT2.0 and *IRIS* suggest that type-II spicules pre-exist at temperatures visible in Lyα, and that some of the plasma in these type-II spicules suddenly gets heated to higher, TR temperatures, which is revealed as rapidly propagating linear features in the TR passbands observed by *IRIS* (i.e., network jets). That is, our analysis does not support the interpretation that the speeds are real mass motions but rather suggests that they arise from thermal fronts, which heat the spicular plasma.

Furthermore, we conclude that since type-II spicules seem to have much lower mass flow speeds than the apparent speeds of network jets (which are not mass flows), this may also have implications for estimates of the contributions of spicules to the solar wind mass flux. As discussed in Tian et al. (2014), using a mean jet speed from their sample of 150 km s^{-1} they estimate a spicular contribution to the solar wind of $(2.8–36.4) \times 10^{12}$ g s^{-1} if all of the mass of the network jets contributes to the solar wind. In addition, they acknowledge that the lack of coronal observations of sufficient sensitivity makes it difficult to assess whether the aforementioned rate is a realistic contribution to the solar wind. They concluded that the above mass contribution rate is ≈2–24 times larger than the total mass loss associated with the solar wind (ranging from $(1.2–1.9) \times 10^{12}$ g s^{-1} between solar minimum and solar maximum respectively). Using the same assumptions here, we would argue that by using the conservative Doppler speeds of about 50 km s^{-1} (as measured in the analysis of Rouppe van der Voort et al. (2015) on type-II spicules) as a more realistic measure for the mass upflows in type-II spicules (instead of the apparent speeds of network jets), this would reduce the values to about one-third, i.e., ≈0.6–8 times the total loss rate of the solar wind. However, neither the Tian et al. (2014) values nor these values are accurate estimates of the mass contributing to the solar wind since it is not known what fraction of the spicular mass is heated to million degree temperatures. We need to stress here that addressing the question of spicular contribution to the solar wind in the way of Tian et al. (2014) is complicated by the fact that, just like with coronal heating, the contribution of the spicules may not be limited to just providing mass, but could also include generation and propagation of currents, which can then dissipate in the wind and lead to extra evaporation. Indeed, parabolic profiles usually suggest that the suspended mass comes down. Our observations, with unique temperature coverage and spatiotemporal resolution, support the view presented in De Pontieu et al. (2017), i.e., that network jets are primarily apparent plane-of-the-sky motions arising from enhanced emission of rapidly propagating heating fronts along pre-existing spicules, rather than actual upward mass motions.

5. Conclusion

We observed the occurrence of a type-II spicule in the common FOVs of VAULT2.0 and *IRIS* SJI imagers. The spicule contains Lyα material at lower intensities for about two minutes prior to its counterpart in Si IV and C II (Figures 2 and 3). Once the type-II spicule reaches TR temperatures, it brightens twice within 52 s in all three passbands (Figure 3).

We employed a state-of-the-art 2.5D MHD Bifrost simulation of a type-II spicule (Martínez-Sykora et al. 2017b). According to this model, ambipolar diffusion facilitates the dissipation of electrical currents within the type-II spicules causing the temperature to increase rapidly. The synthesis of observables from this simulation shows precedence of significant emission for Lyα as compared to Si IV emission in the spicule. The rapid temperature changes have an impact on the emissivity of the different ions. Two brightenings in the same spicule arise from two episodes of current dissipation within the spicule.

In conclusion, the precedence of Lyα emission two minutes before the brightening in Si IV 1400 Å and C II 1330 Å points to the existence of a "Lyα counterpart" for the network jets. Our unique observations elucidate the heating process and the morphology of the type-II spicules. De Pontieu et al. (2017) have provided evidence that the speeds of network jets reported by Tian et al. (2014) and Narang et al. (2016) are not true jet speeds and conversely not mass upflows at those speeds. Our analysis of VAULT2.0 observations provides additional evidence in agreement with De Pontieu et al. (2017) and suggests that spicular material pre-exists at chromospheric temperatures as a Lyα spicule. That spicule heats up to TR temperatures due to a rapidly moving heating front which results in the apparent (and not real mass motion) speeds in the form of fast network jets within the same spicule.

ORCID iDs

Georgios Chintzoglou ⓘ https://orcid.org/0000-0002-1253-8882
Bart De Pontieu ⓘ https://orcid.org/0000-0002-8370-952X
Juan Martínez-Sykora ⓘ https://orcid.org/0000-0002-0333-5717
Tiago M. D. Pereira ⓘ https://orcid.org/0000-0003-4747-4329
Angelos Vourlidas ⓘ https://orcid.org/0000-0002-8164-5948

References

Carlsson, M., & Leenaarts, J. 2012, A&A, 539, A39

Cavallini, F. 2006, SoPh, 236, 415

Chintzoglou, G., Vourlidas, A., Savcheva, A., et al. 2017, ApJ, 843, 93

De Pontieu, B., Hansteen, V. H., McIntosh, S. W., & Patsourakos, S. 2009, ApJ, 702, 1016

De Pontieu, B., Martínez-Sykora, J., & Chintzoglou, G. 2017, ApJL, 849, L7

De Pontieu, B., McIntosh, S. W., Carlsson, M., et al. 2007, Sci, 318, 1574

De Pontieu, B., Title, A. M., Lemen, J. R., et al. 2014, SoPh, 289, 2733

Gudiksen, B. V., Carlsson, M., Hansteen, V. H., et al. 2011, A&A, 531, A154

Hansteen, V. H., Hara, H., De Pontieu, B., & Carlsson, M. 2010, ApJ, 718, 1070

Hayek, W., Asplund, M., Carlsson, M., et al. 2010, A&A, 517, A49

Korendyke, C. M., Vourlidas, A., Cook, J. W., et al. 2001, SoPh, 200, 63

Lemen, J. R., Title, A. M., Akin, D. J., et al. 2012, SoPh, 275, 17

Martínez-Sykora, J., De Pontieu, B., Carlsson, M., et al. 2017a, ApJ, 847, 36

Martínez-Sykora, J., De Pontieu, B., Carlsson, M., & Hansteen, V. 2016, ApJL, 831, L1

Martínez-Sykora, J., De Pontieu, B., & Hansteen, V. 2012, ApJ, 753, 161

Martínez-Sykora, J., De Pontieu, B., Hansteen, V. H., et al. 2017b, Sci, 356, 1269

Milkey, R. W., & Mihalas, D. 1973, ApJ, 185, 709

Narang, N., Arbacher, R. T., Tian, H., et al. 2016, SoPh, 291, 1129

Pereira, T. M. D., De Pontieu, B., Carlsson, M., et al. 2014, ApJL, 792, L15

Pereira, T. M. D., & Uitenbroek, H. 2015, A&A, 574, A3

Pesnell, W. D., Thompson, B. J., & Chamberlin, P. C. 2012, SoPh, 275, 3

Rathore, B., & Carlsson, M. 2015, ApJ, 811, 80

Rouppe van der Voort, L., De Pontieu, B., Pereira, T. M. D., Carlsson, M., & Hansteen, V. 2015, ApJL, 799, L3

Rutten, R. J., Hammerschlag, R. H., Bettonvil, F. C. M., Sütterlin, P., & de Wijn, A. G. 2004, A&A, 413, 1183

Scharmer, G. B., Bjelksjo, K., Korhonen, T. K., Lindberg, B., & Petterson, B. 2003, Proc. SPIE, 4853, 341

Scharmer, G. B., Narayan, G., Hillberg, T., et al. 2008, ApJL, 689, L69

Sukhorukov, A. V., & Leenaarts, J. 2017, A&A, 597, A46

Tian, H., DeLuca, E. E., Cranmer, S. R., et al. 2014, Sci, 346, 1255711

Tsuneta, S., Ichimoto, K., Katsukawa, Y., et al. 2008, SoPh, 249, 167

Uitenbroek, H. 2001, ApJ, 557, 389

Vourlidas, A., Beltran, S. T., Chintzoglou, G., et al. 2016, JAI, 5, 1640003